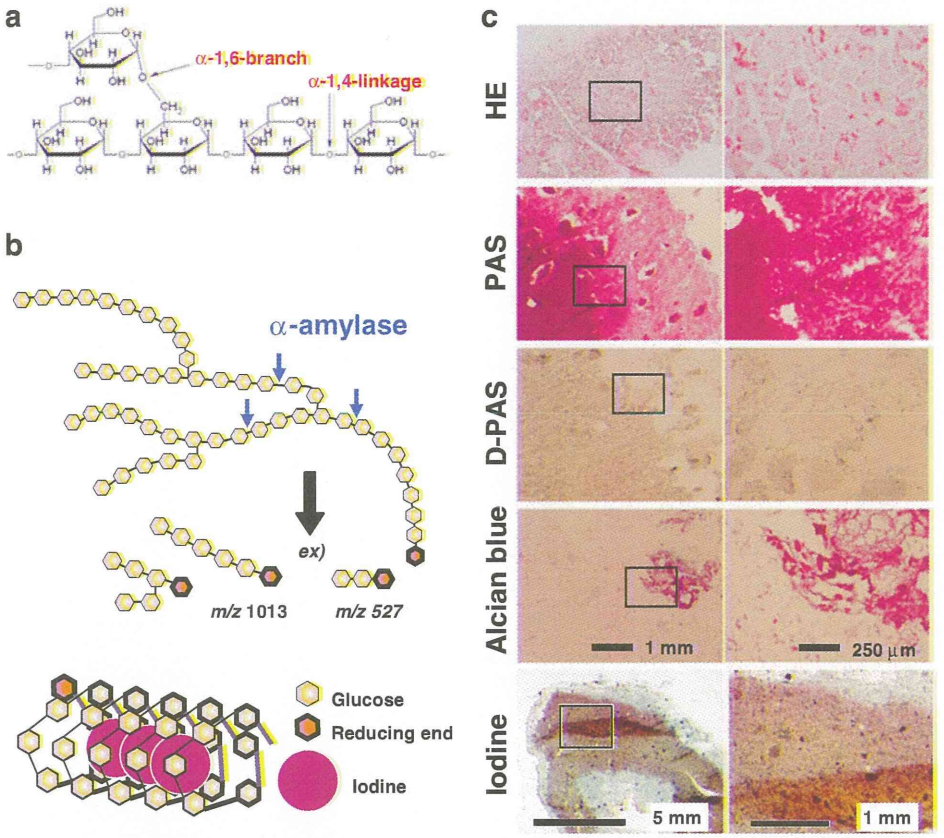

Fig. 6 Reaction of the paraffin sections of the foreign body with iodine. **a** Structure of the α-1,4-linkages and the α-1,6-branch of glucose oligosaccharides. **b** Schematic representation of the enzyme digestion of glucose polysaccharide by α-amylase and the iodide reaction in spires of polysaccharide with α-1,4-linkages. The drawing sizes of the molecules do not reflect the actual ones. **c** Histopathological staining of the paraffin sections of the foreign body. Results of hematoxylin and eosin (*HE*), periodical acid-Schiff (*PAS*), PAS diastase treatment (*D-PAS*), Alcian blue, and iodine stainings are shown. The *right panels* show fourfold magnified images of the respective left panel. In the iodine reaction, *light brown to red purple colors* indicate the presence of oligosaccharide or starch. The strong brown color may be due to the overlap of the sections. The *right panel* shows fourfold magnified image of the boxed region of the left panel

corresponded to the sodium adduct of a polysaccharide having 16 glucose residues (Figs. 2 and 4 and Table 1).

Tandem mass spectrometry of polyglucose in the histopathological paraffin sections

We further investigated the obstruction material using tandem MS (MS*n*) to confirm that the fragment ions were derived from oligosaccharides. First, the direct MS/MS spectrum of the precursor ion at *m/z* 527 was analyzed. The value of *m/z* was identical to that of the sodiated oligosaccharide. In the MALDI-MS/MS experiments using the Mass Microscope, the degradation of carbohydrates formed ion series that included B- and Y-type ion cleavages (nomenclature system of [24]). These ion series are formed by the subsequent loss of the incremental mass of monosaccharides; thus, the ion series for amylose showed a mass difference of 162. We identified the one (C or Y) series oligosaccharides represented by 2-mer ions at *m/z* 203 ($C_6H_{12}O_6$, $[M + Na]^+$) and 3-mer at *m/z* 365 ($C_{12}H_{22}O_{11}$, $[M + Na]^+$; Fig. 5a, b). These results suggest that maltotriose signal with sodium ion ($C_{36}H_{66}O_{33}$, $[M + Na]^+$) was detected as ion at *m/z* 527. Peaks derived from a second (B or Z) series ions were also detected as ions at *m/z* 185, *m/z* 347, and at *m/z* 509 (Fig. 5a, b).

In a similar manner, we detected the direct MS/MS spectrum of the precursor ion at *m/z* 1,013, which was also expected to be a sodiated oligosaccharide. The glucose polymer comprises 5-mer oligosaccharides with sodium ion as a C- or Y-type fragment ion ($C_{30}H_{50}O_{25}$, $[M + Na]^+$, *m/z* 851); the B- or Z-type fragment ions ($C_{30}H_{48}O_{24}$, $[M + Na]^+$, *m/z* 833) were detected along with maltotriose as their ion $[M + Na]^+$ located at *m/z* 527. Thus, the ions of the diagnostic fragments suggest that the ion at *m/z* 1,013 and 527 originate from a polysaccharide or an oligosaccharide (Fig. 5).

Identification of oligosaccharides as a glucose polymer

The *m/z* value of 162 is equivalent to that of dehydrated hexose. If the polymers consisted of α-(1-4)-D-glycopyranosyl units, the main component could be starch and/or glycogen. Such polyglucose sometimes contains α-(1-6)-D-glycopyranosyl branching, as illustrated in Fig. 6a.

We could not assume from the HE staining what would be the component. To confirm the existence of oligosaccharides, we performed conventional histopathological staining of the foreign body (Fig. 6b). PAS staining, used for the detection of sugar or glycogen in the tissue [21], gave strong signals. The PAS-positive signals disappeared after D-PAS treatment (Fig. 6b). These results of PAS staining confirmed the presence of glycogen or other carbohydrate substances. Alcian blue staining, which is usually used for mucin polysaccharide detection, showed weak and irregular signals partly throughout the whole region (Fig. 6c). Following multiple special stainings, Kossa staining for bone, Dylon and Congo red staining for amyloid, S100 for protein, CD68 for human macrophages [22], and silver impregnation for fabric were performed; all of the results were negative (data not shown). Finally, we performed iodine staining. The section was colored brown to red purple and the outside was translucent (Fig. 6c), which indicate the presence of oligosaccharide or starch. In the reaction, iodine colors inside the polysaccharide chain with α-1,4-linkages to the number of the spires. Amylose (only α-1,4-linkages) colors deep blue to purple. Amylopectin has approximately 4% α-(1-6)-D-glycopyranosyl branching. Glycogen has a higher frequency of branches and shorter length than amylopectin. The outer portions of this material appeared translucent, probably because the amylose chain was less than 12 residues in length due to the digestive action in the intestine. The iodide reaction also supported that the foreign material was *mochi*.

Conclusions

With direct MALDI-TOF MS imaging, we identified *mochi* as the obstructing material in small intestinal obstruction. The results in this study indicate that IMS is a very rapid and accurate technique with high sensitivity for the direct analysis of histopathological samples. This is the first case of the identification of oligosaccharides as the main components of histopathological samples using direct MS analyses. MALDI-TOF MS in combination with enzyme digestion will provide support for histopathological study.

Acknowledgments We thank Hosaka K, Saitou A, and Tarumi T for their assistance. We also thank Prof. Sugimura and lab members. This study is supported by Research Grants for PRESTO and SENTAN from Japan Science and Technology Agency to I. Yao.

References

1. Yao I, Sugiura Y, Matsumoto M, Setou M (2008) In situ proteomics with imaging mass spectrometry and principal component analysis in the Scrapper-knockout mouse brain. Proteomics 8 (18):3692–3701
2. Sugiura Y, Setou M (2010) Imaging mass spectrometry for visualization of drug and endogenous metabolite distribution: toward in situ pharmacometabolomes. J Neuroimmune Pharmacol 5 (1):31–43. doi:10.1007/s11481-009-9162-6
3. Bernier UR, Kline DL, Barnard DR, Schreck CE, Yost RA (2000) Analysis of human skin emanations by gas chromatography/mass spectrometry. 2. Identification of volatile compounds that are candidate attractants for the yellow fever mosquito (*Aedes aegypti*). Anal Chem 72(4):747–756
4. Garrett TJ, Yost RA (2006) Analysis of intact tissue by intermediate-pressure MALDI on a linear ion trap mass spectrometer. Anal Chem 78(7):2465–2469
5. Drexler DM, Garrett TJ, Cantone JL, Diters RW, Mitroka JG, Prieto Conaway MC, Adams SP, Yost RA, Sanders M (2007) Utility of imaging mass spectrometry (IMS) by matrix-assisted laser desorption ionization (MALDI) on an ion trap mass spectrometer in the analysis of drugs and metabolites in biological tissues. J Pharmacol Toxicol Methods 55(3):279–288
6. Shimma S, Sugiura Y, Hayasaka T, Hoshikawa Y, Noda T, Setou M (2007) MALDI-based imaging mass spectrometry revealed abnormal distribution of phospholipids in colon cancer liver metastasis. J Chromatogr 855(1):98–103
7. Stoeckli M, Chaurand P, Hallahan DE, Caprioli RM (2001) Imaging mass spectrometry: a new technology for the analysis of protein expression in mammalian tissues. Nat Med 7(4):493–496
8. Setou M, Heeren RM, Stoeckli M, Simma S, Matsumoto M (2007) Mass microscopy. Seikagaku 79(9):874–879
9. Rubakhin SS, Churchill JD, Greenough WT, Sweedler JV (2006) Profiling signaling peptides in single mammalian cells using mass spectrometry. Anal Chem 78(20):7267–7272
10. Luxembourg SL, Mize TH, McDonnell LA, Heeren RM (2004) High-spatial resolution mass spectrometric imaging of peptide and protein distributions on a surface. Anal Chem 76(18):5339–5344
11. Cooks RG, Ouyang Z, Takats Z, Wiseman JM (2006) Detection technologies. Ambient mass spectrometry. Science (New York, NY) 311(5767):1566–1570
12. Sugiura Y, Shimma S, Setou M (2006) Two-step matrix application technique to improve ionization efficiency for matrix-assisted laser desorption/ionization in imaging mass spectrometry. Anal Chem 78(24):8227–8235
13. Shimma S, Sugiura Y, Hayasaka T, Zaima N, Matsumoto M, Setou M (2008) Mass imaging and identification of biomolecules with MALDI-QIT-TOF-based system. Anal Chem 80 (3):878–885
14. Landgraf RR, Garrett TJ, Calcutt NA, Stacpoole PW, Yost RA (2007) MALDI-linear ion trap microprobe MS/MS studies of the effects of dichloroacetate on lipid content of nerve tissue. Anal Chem 79(21):8170–8175
15. Shimma S, Furuta M, Ichimura K, Yoshida Y, Setou M (2006) A novel approach to in situ proteome analysis using a chemical inkjet printing technology and MALDI-QIT-TOF tandem mass spectrometer. J Mass Spectrom Soc Japan 54:133–140
16. Groseclose MR, Andersson M, Hardesty WM, Caprioli RM (2007) Identification of proteins directly from tissue: in situ tryptic digestions coupled with imaging mass spectrometry. J Mass Spectrom 42(2):254–262
17. Walch A, Rauser S, Deininger SO, Hofler H (2008) MALDI imaging mass spectrometry for direct tissue analysis: a new frontier for molecular histology. Histochem Cell Biol 130(3):421–434

18. Caprioli RM, Farmer TB, Gile J (1997) Molecular imaging of biological samples: localization of peptides and proteins using MALDI-TOF MS. Anal Chem 69(23):4751–4760
19. Morita Y, Ikegami K, Goto-Inoue N, Hayasaka T, Zaima N, Tanaka H, Uehara T, Setoguchi T, Sakaguchi T, Igarashi H, Sugimura H, Setou M, Konno H (2009) Imaging mass spectrometry of gastric carcinoma in formalin-fixed paraffin-embedded tissue microarray. Cancer Sci 101(1):267–273
20. Ushijima M, Miyata S, Eguchi S, Kawakita M, Yoshimoto M, Iwase T, Akiyama F, Sakamoto G, Nagasaki K, Miki Y, Noda T, Hoshikawa Y, Matsuura M (2007) Common peak approach using mass spectrometry data sets for predicting the effects of anticancer drugs on breast cancer. Cancer Inform 3:285–293
21. Gahrton G (1964) Microspectrophotometric quantitation of the periodic acid-Schiff (PAS) reaction in human neutrophil leukocytes based on a model system of glycogen microdroplets. Exp Cell Res 34:488–506
22. Holness CL, Simmons DL (1993) Molecular cloning of CD68, a human macrophage marker related to lysosomal glycoproteins. Blood 81(6):1607–1613
23. Hayasaka T, Goto-Inoue N, Ushijima M, Yao I, Yuba-Kubo A, Wakui M, Kajihara S, Matsuura M, Setou M (2011) Development of imaging mass spectrometry (IMS) dataset extractor software, IMS convolution. Anal Bioanal Chem 401:183–193
24. Domon B, Costello CE (1988) Structure elucidation of glycosphingolipids and gangliosides using high-performance tandem mass spectrometry. Biochemistry 27(5):1534–1543

Loss of lymphatic vessels and regional lipid accumulation is associated with great saphenous vein incompetence

Hiroki Tanaka, MD,[a,b,c] Nobuhiro Zaima, PhD,[b,d] Takeshi Sasaki, PhD,[c] Naoto Yamamoto, MD,[a,c] Masaki Sano, MD,[a,c] Hiroyuki Konno, MD,[c] Mitsutoshi Setou, MD,[b] and Naoki Unno, MD,[a,c] *Hamamatsu and Nara, Japan*

Objective: Recent studies suggest that biologic changes in the vein wall associated with varicose veins (VVs) occur not only in valvular tissue but also in nonvalvular regions. We previously used imaging mass spectrometry (IMS) to determine the distribution of lipid molecules in incompetent valve tissue. In this study, we used IMS to analyze incompetent great saphenous veins (GSVs) in patients with varicose vein (VV) to assess the distribution of lipid molecules.

Methods: We obtained GSV tissue from 38 VV patients (50 limbs) who underwent GSV stripping. For the control veins (CV), we obtained GSV samples from 10 patients undergoing infrainguinal bypass with reversed GSV grafting for peripheral artery occlusive disease (10 limbs). Conventional and immunofluorescence staining were performed for histopathologic examination. The total lipid content in the homogenized vein tissue was determined. The localization of each lipid molecule in the vein wall was assessed by IMS.

Results: The histologic examination showed the VV walls were significantly thicker than the CV walls, and only the VV adventitia was positive for lipid staining. The VV wall had higher concentrations of phospholipids and triglycerides than the CV wall. IMS revealed an abnormal accumulation of lysophosphatidylcholine (LPC; 1-acyl 16:0) and phosphatidylcholine (diacyl 16:0/20:4) in the VV intima and media. Triglyceride was found only in VV adventitia. The number of lymphatic vessels, as measured by staining with D2-40, a lymphatic vessel-specific marker, was significantly lower in the VV adventitia than in the CV adventitia. Lymphatic vessel reduction may be associated with insufficient lymphatic drainage in the VV adventitia causing histologic changes in VV tissue.

Conclusions: The accumulation of LPC (1-acyl 16:0) and PC (diacyl 16:0/20:4) in the VV intima and media may be associated with chronic inflammation, leading to VV tissue degeneration. Furthermore, insufficient lipid drainage by lymphatic vessel may be responsible for accumulation of lipid molecules and subsequent vein wall degeneration. (J Vasc Surg 2012;55:1440-8.)

Clinical Relevance: Abnormal distribution of lipid molecules in varicose vein (VV) tissue in patients at CEAP class C_{2-3} and C_{4-5} suggests that VV-associated accumulation of lipid molecules begins in the early clinical stages of the disease and continues through the advanced stages. In particular, the accumulation of both lysophosphatidylcholine (1-acyl 16:0) and phosphatidylcholine (diacyl 16:0/20:4) in the media was significantly higher in VV tissue from patients in advanced clinical stages, suggesting an association between lipid accumulation and chronic inflammation of skin and subcutaneous tissues. Further study is needed to clarify the effect of lymph stasis on VVs and chronic inflammation. The mechanism whereby adventitial lymphatic vessels are damaged is also unknown. Consistent venous hypertension and subsequent overload to the lymphatics may account for the lymphatic damage. In addition, accumulation of possible proinflammatory lipid molecules in VV walls may further damage the adventitial lymphatic vessels.

We previously determined the characteristic distribution of lipid molecules in regions surrounding incompetent valves in patients with varicose veins (VVs) by using imaging mass spectrometry (IMS).[1] IMS revealed the accumulation of lysophosphatidylcholine (LPC; 1-acyl 16:0) and phosphatidylcholine (PC; diacyl 16:0/20:4) in the valvular region. Because these molecules are potential proinflammatory lipids,[2-4] this finding suggests that LPC and PC are involved in the development of tissue inflammation and valvular incompetence. These results support previously reported data.[5,6] However, recent studies suggest that histologic changes in the wall of the great saphenous vein (GSV) may precede valvular dysfunction.[5] The pathogenesis of these biologic changes is yet to be elucidated. Investigation of the lipid profile of the GSV wall may help gain insight into the influence of dyslipidemia in the VV tissues. For this purpose, we used IMS to analyze the

From the Division of Vascular Surgery,[a] the Department of Cell Biology and Anatomy Systems Molecular Anatomy,[b] the Second Department of Surgery,[c] and the Department of Anatomy,[c] Hamamatsu University School of Medicine, Hamamatsu; and the Department of Applied Biological Chemistry, Kinki University, Nara.[d]

This study was supported by Grant-in-Aid for Scientific Research (C) from the Japan Society for the Promotion of Science (NU).

Author conflict of interest: none.

Presented at the Twenty-third Annual Meeting of the American Venous Forum, San Diego, Calif, February 23-26, 2011.

Reprint requests: Naoki Unno, Division of Vascular Surgery, Hamamatsu University School of Medicine, 1-20-1 Handayama, Higashi-ku, Hamamatsu 431-192, Japan. (e-mail: unno@hama-med.ac.jp).

The editors and reviewers of this article have no relevant financial relationships to disclose per the JVS policy that requires reviewers to decline review of any manuscript for which they may have a competition of interest.

0741-5214/$36.00

doi:10.1016/j.jvs.2011.09.064

Table I. Demographic and clinical data for each group of patients

Variable[a]	*Control veins*	C_{2-3}	C_{4-5}
Limbs	10	27	23
Sex			
Men	9	5	4
Women	1	17	12
Age, years	65.9 ± 11.4	62.8 ± 13.8	64.7 ± 15.1
Disease duration, years	. . .	13.4 ± 11.7	17.8 ± 16.9
Cholesterol, mg/dL			
Total	191.3 ± 43.3	186.7 ± 41.9	182.2 ± 45.2
LDL	121.3 ± 22.7	116.6 ± 31.6	117.5 ± 34.2
HDL	39.2 ± 15.2	43.1 ± 12.8	41.0 ± 12.3
Triglyceride, mg/dL	108.3 ± 51.2	113.1 ± 24.1	112.5 ± 32.2
Hemoglobin A_{1C}, %	6.0 ± 1.9	5.9 ± 1.2	5.8 ± 2.5

HDL, High-density lipoprotein; *LDL*, low-density lipoprotein.
Categoric data are expressed as number and continuous data as mean ± standard deviation.

distribution of lipid molecules in incompetent GSVs in VV patients.

METHODS

All procedures used in this study were approved by the Ethics Committee of Clinical Research of the Hamamatsu University School of Medicine.

Sample collection. We enrolled 48 patients in this study between April 2008 and December 2010. We obtained GSV tissue from of 38 VV patients (50 limbs) who underwent GSV stripping. Clinical information is summarized in Table I. By CEAP clinical severity scores,[7] 16 samples were assigned to C_2 (simple VV), 11 to C_3 (VV with ankle swelling), 21 to C_4 (VV with skin changes), and 2 to C_5 (VV with healed ulcer). To investigate the association between the tissue lipid profiles and disease severity, we classified the VV patients into two groups: C_{2-3} (moderate VV group) and C_{4-5} (severe VV group). As control veins (CV), segmental GSV tissues were harvested from 10 patients (10 limbs) with peripheral artery occlusive disease who underwent infrainguinal bypass with reversed GSV grafting (Table I).

To maintain tissue morphology and minimize molecular degradation, tissue samples were immediately frozen in liquid nitrogen and stored at −80°C until matrix-assisted laser desorption–ionization IMS (MALDI-IMS) analysis; other samples were preserved in 10% formalin for histopathologic examination.

All patients underwent duplex ultrasound scans with a 7.5-MHz transducer (LOGIC 500; GE Yokogawa Medical, Tokyo, Japan) to assess venous hemodynamics. Clinical disease severity was graded using the standard CEAP classification according to the recommendations of an International Consensus Committee on Chronic Venous Disease.[7] Venodynamic studies were performed using duplex scanning, with patients scanned while standing to assess reflux throughout the GSV. Reflux was defined as flow in the reverse direction of the physiologic flow of duration >0.5 seconds after a provocation maneuver.[8] All VV patients had retrograde flow in the saphenofemoral junction; the control patients had no reflux in the GSV. We analyzed the GSV tissue that was in close to the saphenofemoral junction, excluding the terminal valve.

Imaging mass spectrometry. We cut the frozen tissues into 8-μm-thick longitudinal sections using a cryostat (CM1950; Leica, Wetzler, Germany). Sections were thaw-mounted onto indium tin oxide–coated glass slides (Bruker Daltonics, Bremen, Germany) and dried at room temperature. A total of 500 μL of 2,5-dihydroxybenzoic acid solution (50 mg/mL in methanol/water, 7:3 [v/v]) was sprayed on the sample sections using a 0.2-mm nozzle airbrush (Procon Boy FWA Platinum; Mr. Hobby, Tokyo, Japan). A 15-cm distance was maintained between the nozzle and the tissue surface during spraying.

We performed IMS using a MALDI time of flight (TOF)/TOF-type instrument (Ultraflex II TOF/TOF; Bruker Daltonics, Bremen, Germany) equipped with a 355-nm neodymium-doped yttrium aluminium garnet laser (repetition rate, 200 Hz). Data were acquired with a step size of 50 μm for the samples in the positive ion mode (reflector mode). The mass spectrometer parameters were set to obtain the highest sensitivity with mass/charge ratio (*m/z*) values of 400 to 1000. All spectra were acquired automatically using Flex Imaging software (Bruker Daltonics). The laser was used to irradiate each position 100 times. The peaks were normalized to the total ion current and then compared. Ion images were created using Flex Imaging software (Bruker Daltonics).

Tandem MS. Tandem MS (MS/MS) was performed on tissue sections using a linear quadruple ion trap LTQ-XL mass spectrometer (Thermo Fisher Scientific, Waltham Mass), as described previously.[9] Precursor and fragment ions obtained by collision-induced dissociation were ejected from the ion trap and analyzed. Collision energy was set to 30% (this unit is customized for LTQ-XL; 100% indicates the energy that completely fragments the peptide Met-Arg-Phe-Ala). The laser energy was set to 30 μJ. Specific fragment patterns of triglycerides (TGs), LPC, and PC were confirmed using previous reports.[1,3,10-12]

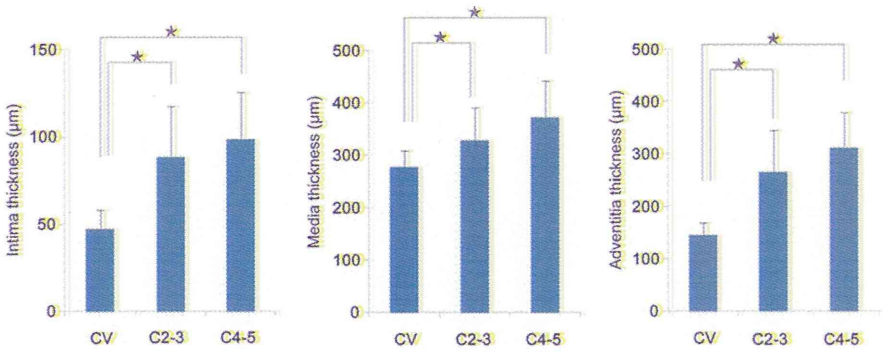

Fig 1. Thickness of the great saphenous vein wall. The measured thickness of the **(left)** intima, **(middle)** media, and **(right)** adventitia layers is compared among the control vein (*CV*) and varicose veins from the CEAP C_{2-3} and C_{4-5} groups. $*P < .05$ indicates a statistically significant difference. The *error bars* show the standard deviation.

Histopathologic examinations. Specimens for light microscopy were fixed in 10% neutral-buffered formalin solution and were processed to prepare 4-mm-thick paraffin sections. Sections were stained with hematoxylin and eosin (HE) and elastica van Gieson (EVG). A light microscope was used for quantitative measurements.

Biochemical quantitation. Total lipids were extracted from homogenized tissue as described previously.[13] Phospholipids and TGs were quantified using colorimetric methods (Wako, Osaka, Japan).

Immunostaining. Tissue sections (8 μm) were fixed with 4% paraformaldehyde in phosphate-buffered saline (pH 7.4) for 10 minutes at room temperature. Sections were rinsed with phosphate-buffered saline, preincubated with 10% normal goat serum (Nichirei Biosciences, Tokyo, Japan), and incubated overnight at 4°C with rabbit anti-von Willebrand factor (1:400; Acris Antibodies GmbH, Herford, Germany) and mouse anti-D2-40 (1:200; Acris Antibodies GmbH, Herford, Germany). Immunoreactivity was visualized using Alexa Fluor 488-conjugated antirabbit immunoglobulin G and Alexa Fluor 594-conjugated anti-mouse immunoglobulin G (Molecular Probes; Invitrogen, Carlsbad, Calif). All Alexa Fluor-conjugated secondary antibodies were diluted 200-fold for use. The slides were mounted in a glycerol-based Vectashield medium (Vector Laboratories, Burlingame, Calif) containing the nucleus staining reagent 4′,6-diamidino-2-phenylindole.

Statistical analysis. Results have been summarized using descriptive statistics. All data are expressed as mean ± standard deviation. The significance of the differences between groups with respect to vein wall thickness, lipid content, ratio of intensity, and the number of lymphatic vessels was determined by one-way analysis of variance, followed by the Tukey test. A value of $P < .05$ was considered significant. All statistical analyses were performed with StatView 5.0 software (SAS Institute, Tokyo, Japan).

RESULTS

Clinical information. Patient demographics are reported in Table I. The control and C_{2-3}, and C_{4-5} VV groups did not differ significantly in age, disease duration, serum total cholesterol, serum low-density lipoprotein (LDL), serum high-density lipoprotein (HDL), serum TG contents, and hemoglobin A_{1C}. The only significant difference between groups was the sex ratio.

Histopathologic examinations. The intimal thickness of VV tissue in the C_{2-3} and C_{4-5} groups was 1.9-fold and 2.1-fold greater, respectively, than that in the CV tissue ($P < .01$; Fig 1). The medial thickness of VV tissue in groups C_{2-3} and C_{4-5} was 1.2-fold and 1.3-fold greater, respectively, than that in CV tissue, ($P < .01$; Fig 1). The adventitial thickness of VV tissue in groups C_{2-3} and C_{4-5} was 1.8-fold and 2.1-fold greater, respectively, than that of the CV tissue ($P < .05$; Fig 1).

Lipid staining and quantification. In lipid staining with oil red O, the adventitia of the VV tissue showed positive staining, but other regions, such as the intima and media, were not positively stained (Fig 2, *A*). In contrast, no regions of the CV tissue showed positive staining (Fig 2, *A*). These results suggested an unknown mechanism of lipid accumulation in the adventitial tissue of the VV tissue. The PL content in groups C_{2-3} and C_{4-5} was higher by 1.8-fold and 1.7-fold, respectively, than in CV tissue ($P < .01$; Fig 2, *B*). In addition, the TG content in groups C_{2-3} and C_{4-5} was higher by 2.1-fold and 2.5-fold, respectively, than in the CV tissue ($P < .01$; Fig 2, *B*). The experimental groups did not differ in PL and TG contents (Fig 2, *B*).

Imaging mass spectrometry. We investigated the distribution pattern of lipids in CV and VV tissues using MALDI-IMS (Fig 3, *A*). On gross inspection, there was no notable difference in the patterns between the control and VV groups. Among the spectrum patterns, we paid attention to seven peaks: m/z 496, 782, 798, 804, 820, 879, and 881, which were determined to correspond to LPC (1-acyl 16:0) + H, PC (diacyl 16:0/18:1) + Na, PC (diacyl 16:0/18:1) + K, PC (diacyl 16:0/20:4) + K, TG (52:3) + K and TG (52:2) + K, respectively, based on MS/MS and previous reports using IMS (Table II).

Further analysis using MALDI-IMS revealed that the distribution of LPC (1-acyl 16:0), PC (diacyl 16:0/20:4),

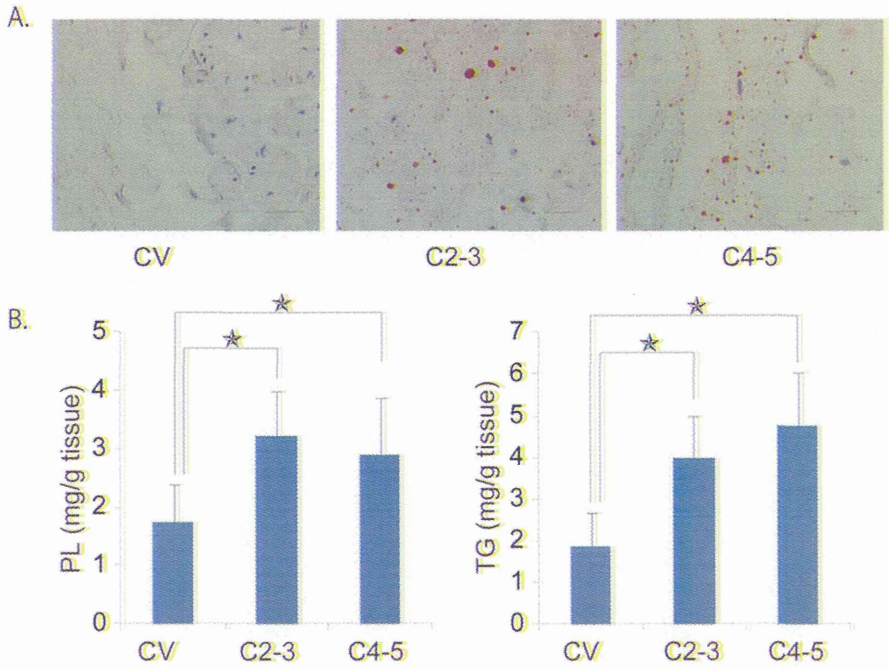

Fig 2. Lipid staining and quantification in vein walls. **A,** Oil red O staining (*bar* = 20 μm). **B,** Lipid content in vein tissue. The phospholipid (*PL*) and triglyceride (*TG*) content of vein walls were compared among the control vein (*CV*) and varicose veins from the CEAP C_{2-3} and C_{4-5} groups. $*P < .05$ indicates a statistically significant difference. The *error bars* show the standard deviation.

TG (52:3), and TG (52:2) in VV tissue differed between each tissue, whereas PC (diacyl 16:0/18:1) was detected ubiquitously in all tissues (Fig 3, *B*). Accumulation of LPC (1-acyl 16:0) and PC (diacyl 16:0/20:4) was found in the VV intima and media. In contrast, accumulation of TG (52:3) and TG (52:2) was found in VV adventitia. However, the distribution patterns of LPC (1-acyl 16:0), PC (diacyl 16:0/20:4), and TG (52:3) and TG (52:2) were similar in the two experimental groups (Fig 3, *B*).

Fig 3, *C* shows quantitative comparisons of LPC (1-acyl 16:0), PC (diacyl 16:0/18:1), PC (diacyl 16:0/20:4), and TG (52:3) and TG (52:2) in the intima, media, and adventitia between CV, C_{2-3} and C_{4-5} tissue as expressed to be a ratio of relative intensity (RRI). RRI was calculated as follows. We designated the intima, media, and adventitia in the region analyzed by IMS as covering the total of ion intensities. The ion intensity obtained from each tissue was not the absolute value. Therefore, each molecule's ion intensity was standardized to that of PC (16:0/18:1) as expressed to be a RRI. PC (16:0/18:1) was widely available for the internal standard molecule at mammalian tissue analysis by IMS.

There were no differences in the RRIs for PC (diacyl 16:0/18:1) among these regions (data not shown). In contrast, the RRIs for LPC (1-acyl 16:0) were significantly higher in the intima, media, and adventitia of VV tissues from the C_{2-3} and C_{4-5} groups compared with controls ($P < .05$; Fig 3, *C*). Similarly, the RRIs for PC (diacyl 16:0/20:4) were significantly higher in the intima, media, and adventitia of C_{2-3} and C_{4-5} VV tissues compared with controls ($P < .05$). The RRIs for TG (52:3) and TG (52:2) in the intima and media of VV tissues were not different from those of CV tissues. However, the RRIs for TG (52:3) and TG (52:2) were significantly higher in the adventitia of VV tissues than in controls ($P < .05$). There were no significant differences in the RRIs for TG (52:3) and TG (52:2) in any tissues between the C_{2-3} and C_{4-5} groups (Fig 3, *C*).

Immunostaining. The vascular endothelial marker von Willebrand factor and a marker specific for lymphatic vessels (D2-40) were applied to the control and VV tissues for visualization of lymphatic vessels. Immunofluorescence staining revealed that lymphatic vessels were present in the adventitia of the GSV in controls and VV tissues (Fig 4, *A*). Significantly fewer lymphatic vessels were seen in complete circumferential sections in the VV groups (C_{2-3} and C_{4-5}) than in controls ($P < .05$; Fig 4, *B*).

DISCUSSION

In this study, the histopathologic changes in structural components of the intima and media (such as collagen, elastin, and smooth muscle) of incompetent GSVs from VV patients are comparable to those previously reported.[14-17] It has been suggested that these changes are due to chronic inflammation in the vein tissue.[14,18-20] Although we showed the increased wall thickness according to the ad-

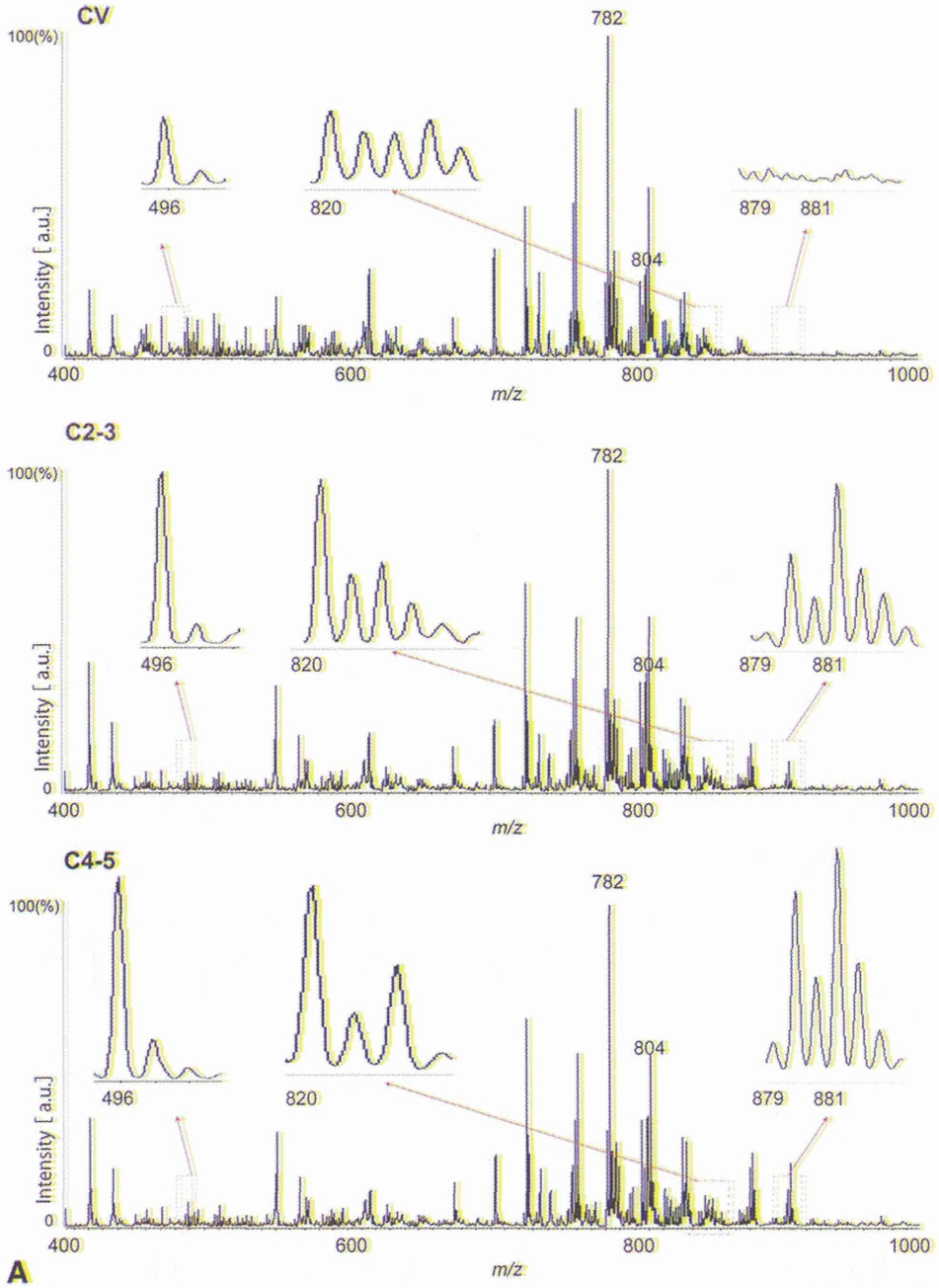

Fig 3. Lipid content analyses by mass spectrometry. **A,** Representative mass spectrum pattern and spectrum of assigned molecule. **B,** Imaging mass spectrometry of vein tissue (*bar* = 200 μm). **C,** The ratio of intensity in vein tissues was compared among control veins (*CV*) and varicose veins from the CEAP $C_{2\text{-}3}$ and $C_{4\text{-}5}$ groups by one-way analysis of variance, followed by the Tukey test. $^{*}P < .05$ indicates a statistically significant difference. $^{\dagger}P < .05$ indicates a statistically significant difference between the $C_{2\text{-}3}$ and $C_{4\text{-}5}$ varicose vein groups. The *error bars* show the standard deviation.

vanced clinical stages, it may be better to use the ratio between the vein wall thickness and the diameter, because wall thickness varies significantly with the size of the vein.

Our previous study was the first to report the abnormal accumulation of lipid molecules in incompetent valve in VVs.[1] In this study, the lipid staining was limited only to the adventitia, and not to the intima and media. We previously reported that lipid staining in the intimal and medial regions was commonly positive in atherosclerotic tissues,[21] which suggested the mechanism of lipid accumulation in

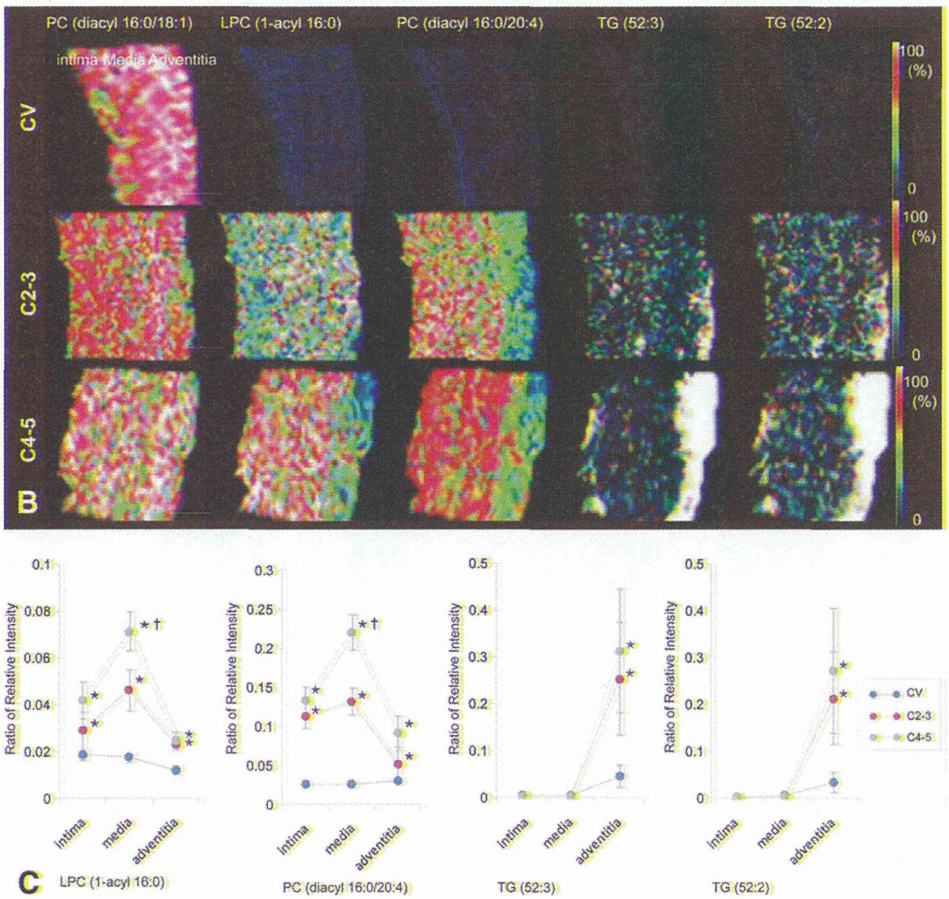

Fig 3. Continued

Table II. Lipid molecule assignments by mass spectrometry

Mass (m)/charge (z)	*Assignment of molecule*
496	LPC (1-acyl 16: 0) + Na
780	PC (diacyl 16:0/18:2) + Na
782	PC (diacyl 16:0/18:1) + Na
796	PC (diacyl 16:0/18:2) + K
798	PC (diacyl 16:0/18:1) + K
804	PC (diacyl 16:0/20:4) + Na
820	PC (diacyl 16:0/20:4) + K
879	Triglyceride (52:3) + K
881	Triglyceride (52:2) + K

LPC, Lysophosphatidylcholine; *PC*, phosphatidylcholine.

the VV tissue seem to be different from that in atherosclerosis. The oil red O staining is a lysochrome diazo dye used for staining of neutral TGs and lipids on frozen sections and some lipoproteins on paraffin sections. To investigate more details of the lipid accumulation and clarify the underlining mechanisms, we applied MALDI-IMS. Unlike conventional biochemical tests that measure lipid content in homogenized tissues or with simple oil red O staining, MALDI-IMS enables the analysis of spatial distributions or specific lipids, along with their fatty acid content, in regions such as the intima, media, and adventitia.

At present, MALDI-IMS is the only method available for the detailed assessment of lipid molecules in tissue. This method distinguishes between different lipid molecular species by simultaneously determining the differences in the mass/charge ratios (m/z).

In the present study, PC (diacyl 16:0/20:4) was elevated in all three layers of VV tissues. Although the range of biochemical effects of PC (diacyl 16:0/20:4) is uncertain, elevated levels of the molecule have been reported in mammalian tissues with chronic inflammation.[3,4] We observed that PC (diacyl 16:0/20:4) contains arachidonic acid, which is a precursor to lipid mediators such as proinflammatory prostaglandins and leukotrienes. Taken together, these data indicate that the elevated tissue content of PC (diacyl 16:0/20:4) may be associated with chronic inflammation in the incompetent GSV.

Other studies have reported the occurrence of chronic inflammation in VV tissue.[6,22] LPC (1-acyl 16:0) is known to be a chemotactic factor for macrophages and lymphocytes as well as an inducer of expression of both vascular cell

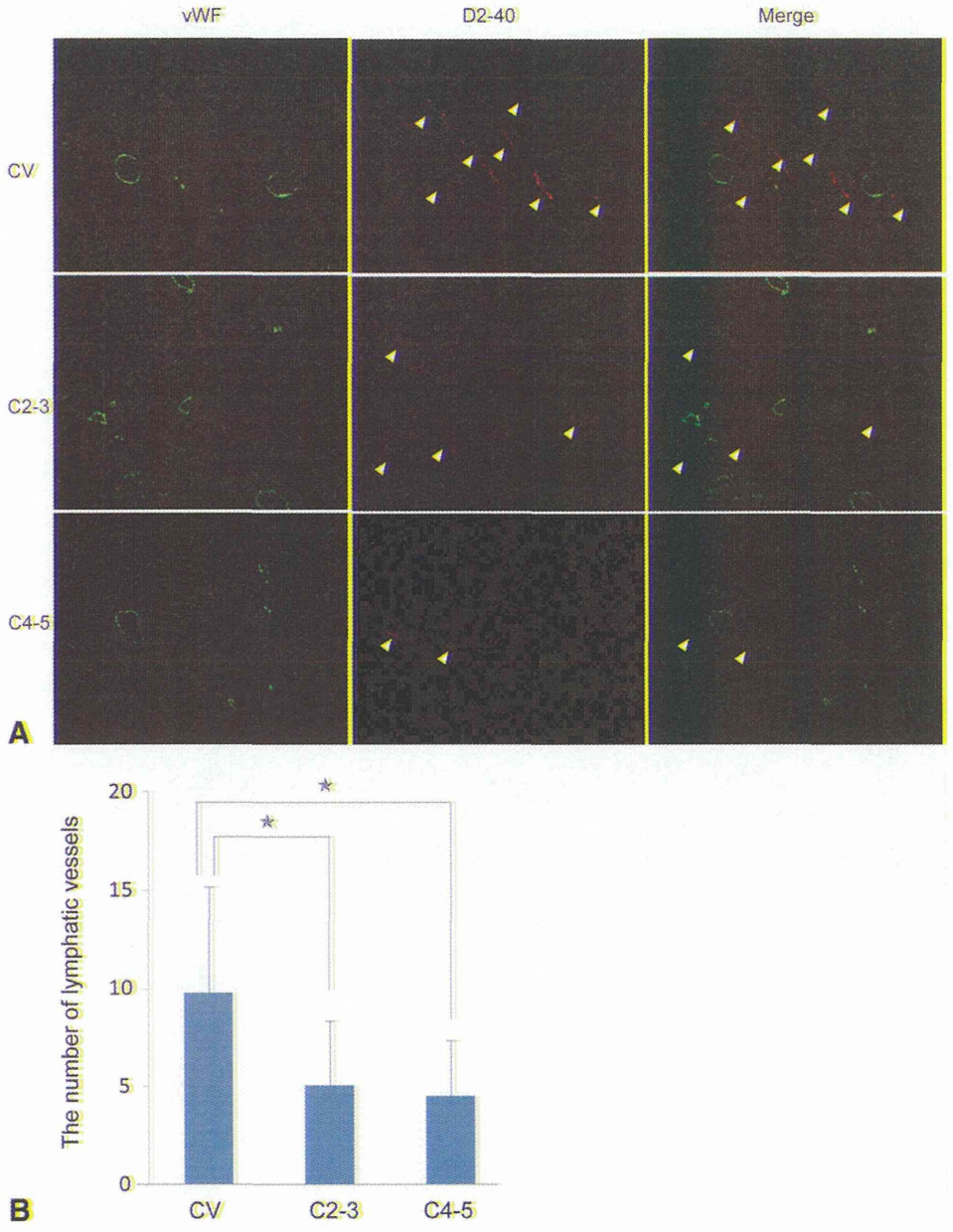

Fig 4. Lymphatic vessel in vein wall. **A,** Immunofluorescent staining for von Willebrand Factor (*green*) and D2-40 (*red; bar* = 20 μm). **B,** Number of lymphatic vessels in complete circumferential sections from each group. $*P < .05$ indicates a statistically significant difference. The *error bars* show the standard deviation.

adhesion molecule-1 and intercellular adhesion molecule-1 in endothelial cells.[23] Therefore, LPC (1-acyl 16:0) may also contribute to the chronic inflammation in VV tissue.

Previous studies have highlighted the histologic changes in the intima and media of VV tissues[24,25]; however, adventitial changes have not been reported. The adventitial triglyceride accumulation in VV tissues revealed by MALDI-IMS in this study sheds light on the pathogenesis of the outer surface of the vein wall, which has been previously overlooked. In Fig. 3, *C*, unlike LPC and PC, TG accumulation was limited to the adventitia of the VV tissue. Although LPC, PC, and TG are all lymph ingredients,[26] LPC and PC are also cellular components.[27,28] Therefore, the elevation of LPC and PC in the intima and media might reflect the increase in the number of inflammatory cells in the regions, and lymph stasis (ie, TG accumulation) might be present only in the adventitial regions.